Characterizing *r*-Process Sites through Actinide Production

Characterizing r-Process Sites through Actinide Production

Erika M. Holmbeck[1,2], Rebecca Surman[1,2], Anna Frebel[3,2], G. C. McLaughlin[4,2], Matthew R. Mumpower[5,6,2], Trevor M. Sprouse[1], Toshihiko Kawano[5], Nicole Vassh[1,2], Timothy C. Beers[1,2]

[1] Department of Physics, University of Notre Dame, Notre Dame, IN 46556, USA
[2] JINA Center for the Evolution of the Elements, USA
[3] Department of Physics and Kavli Institute for Astrophysics and Space Research, Massachusetts Institute of Technology, Cambridge, MA 02139, USA
[4] Department of Physics, North Carolina State University, Raleigh, NC 27695, USA
[5] Theoretical Division, Los Alamos National Laboratory, Los Alamos, NM, 87545, USA
[6] Center for Theoretical Astrophysics, Los Alamos National Laboratory, Los Alamos, NM, 87545, USA

E-mail: eholmbec@nd.edu

November 2019

Abstract. Of the variations in the elemental abundance patterns of stars enhanced with r-process elements, the variation in the relative actinide-to-lanthanide ratio is among the most significant. We investigate the source of these actinide differences in order to determine whether these variations are due to natural differences in astrophysical sites, or due to the uncertain nuclear properties that are accessed in r-process sites. We find that variations between relative stellar actinide abundances is most likely astrophysical in nature, owing to how neutron-rich the ejecta from an r-process event may be. Furthermore, if an r-process site is capable of generating variations in the neutron-richness of its ejected material, then only one type of r-process site is needed to explain all levels of observed relative actinide enhancements.

1. Introduction

The rapid neutron-capture ("r") process is the physical mechanism by which about half the elements heavier than iron in the Solar System were created. The r-process was first identified by [1] and [2], but it is still unclear where the r-process may occur astrophysically. Outside of the Solar System, traces of the r-process lie in very metal-poor ([Fe/H]‡ $= -2$) stars that show an enhancement of the heavy, r-process elements

‡ $[\mathrm{A/B}] = \log(N_A/N_B)_* - \log(N_A/N_B)_\odot$, where N is the number density of an element in the star (*) compared to the Sun ($\odot$).

in their photospheres. Stars with low metallicity indicate few nucleosynthetic events by supernovae that would otherwise release an abundance of iron into the primordial gas of the interstellar medium. In this way, the elemental abundances in low-metallicity stars record the chemical signatures of nucleosynthetic events preceding their formation.

Of metal-poor stars, less than about 20% show an enhancement of r-process elements in their photospheres. The level of r-process enhancement in a star is quantified by the europium ($_{63}$Eu) abundance since Eu in the Solar System was predominantly made by the r-process, and it is one of the easiest elements to observe with high-resolution spectroscopy using ground-based telescopes. The relative level of Eu to Fe abundance in a star is a proxy for how much r-process enhancement preceded the star's formation compared to the chemical evolution of that gas from supernova events. Stars over-enhanced with Eu relative to Fe compared to the Sun are called "r-process enhanced" and are divided into two categories: "r-I," with $0.3 < [\mathrm{Eu/Fe}] \leq 1.0$ (i.e., between a factor of 2 and 10 greater than the Solar value), and "r-II," with $[\mathrm{Eu/Fe}] > 1.0$ (i.e., over a factor of 10 greater than the Solar System). These r-I and r-II stars are relics of prolific r-process event(s) that occurred before the gas was enriched by supernovae, and are therefore considered tracers of nearly pure r-process events.

Scaled to Eu, the relative abundance patterns of the r-I and r-II stars are strikingly similar between the second and third r-process peaks at $(Z, A) \sim (54, 130)$ and $(78, 195)$, respectively. However, large variations exist in the actinide elements ($_{90}$Th and $_{92}$U) and the light r-process elements in the Sr-Y-Zr group ($Z = 38$–40). Figure 1 shows the scaled abundance patterns of several r-II stars as well as the variation across the stars for each element. Stars with an over-abundance of [Th/Eu] relative to the Solar System are considered "actinide-boost" stars, occurring in about 30% of r-process enhanced stars.

1.1. Cosmochronometry

Since the observable actinides, ^{232}Th and ^{238}U, have very long halflives (14.0 Gyr and 4.47 Gyr, respectively), radioactive decay principles can be applied to approximate an age for the material in stars in which both of these elements are observed. Compared to some stable element co-produced by the r-process (typically Eu), the radioactive decay ages can be calculated in three ways:

$$t = 46.67\ \mathrm{Gyr}\left[\log\epsilon\left(\mathrm{Th/Eu}\right)_0 - \log\epsilon\left(\mathrm{Th/Eu}\right)_{\mathrm{obs}}\right] \quad (1)$$

$$t = 14.84\ \mathrm{Gyr}\left[\log\epsilon\left(\mathrm{U/Eu}\right)_0 - \log\epsilon\left(\mathrm{U/Eu}\right)_{\mathrm{obs}}\right] \quad (2)$$

$$t = 21.80\ \mathrm{Gyr}\left[\log\epsilon\left(\mathrm{U/Th}\right)_0 - \log\epsilon\left(\mathrm{U/Th}\right)_{\mathrm{obs}}\right], \quad (3)$$

where $\log\epsilon\left(\mathrm{X/Eu}\right)_0$ is the initial production ratio corresponding to the formation of europium and element X by the r-process at $t = 0$, and $\log\epsilon\left(\mathrm{X/Eu}\right)_{\mathrm{obs}}$ is the ratio derived from observations (present day). By determining the observed ratio from stellar spectra, and assuming some initial production ratio, the time t for which the radioactive element X has decayed can be calculated. If the initial production ratios are a good descriptor of the progenitor r-process site, then all three of these ages should agree to

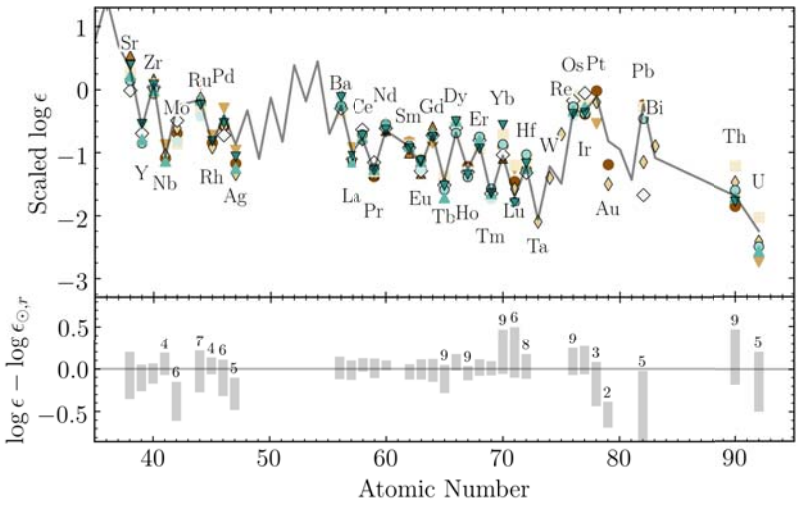

Figure 1. Abundance patterns of 10 r-II stars (CS22892-052 [3], CS22953-003 [4], CS29497-004 [5], CS31082-001 [6], J0954+5246 [7], HE2327-5642 [8], HE2252-4225 [9], J2038−0023 [10], HE1523-0901 [11], and J1538−1804 [12]) scaled to their average difference from the Solar value between Eu and Lu (top), and the range of abundances for each element compared to the Solar System abundance (bottom). Numbers above the ranges in the bottom panel indicate how many stars from the upper panel have a measurement of that element. When not indicated, all 10 stars have a measured abundance.

the same value and be within physical limits (i.e., older than 0 Gyr, but no older than the age of the Universe). Historically, production ratios are used from r-process waiting point calculations or r-process simulations of supernovae [13, 14]. For most r-process enhanced stars, ages calculated with these production ratios are relatively consistent. However, the same calculation with actinide-boost stars yields extremely different ages. Notably, the Th/Eu age (Equation 1) is often negative, unphysically implying that actinide-boost stars are yet to be created. Nevertheless, the U/Th age (Equation 3) consistently produces accurate ages for both actinide-boost and non-actinide-boost stars alike.

1.2. r*-Process Sites*

The recent gravitational wave event GW170817 proved that neutron-star mergers (NSMs) occur in the Universe [15]. Follow-up on the electromagnetic ("kilonova") component to this event revealed evidence that the lanthanide elements were created in the merger, confirming that NSMs are one r-process site [16, 17, 18]. Although lanthanide production was deduced from the event, the extent of actinide production (if any) by NSMs is unknown. In this study, we find initial production ratios from NSM sites and apply those production ratios to investigate whether NSMs may be the source of the actinide-boost phenomenon observed in some r-process enhanced stars.

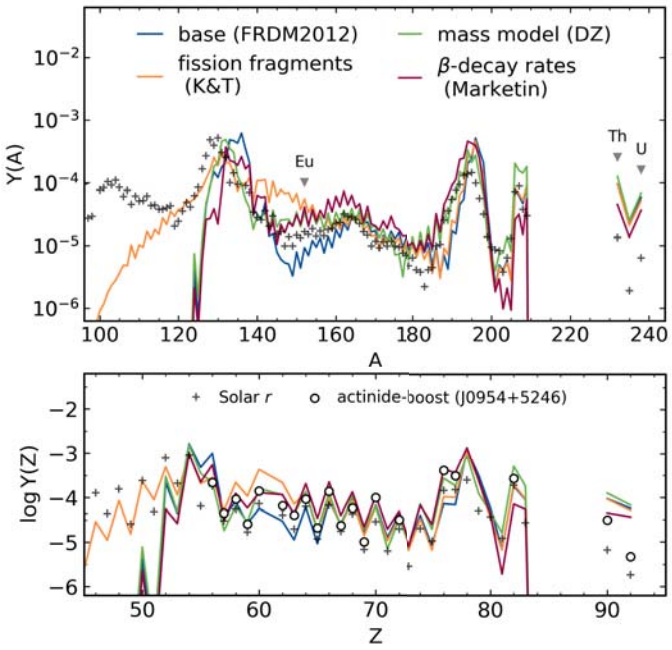

Figure 2. Final isotopic (top) and elemental (bottom) abundance patterns using the four variations on nuclear input described in Section 2. For guidance, the locations of the Eu, Th, and U isotopes are indicated. The scaled abundances for the actinide-boost star J0954+5246 are shown in the lower panel for comparison.

2. Nuclear Physics Uncertainties

In this study, we run nucleosynthesis simulations using the network code Portable Routines for Integrated nucleoSynthesis Modeling (PRISM, [19] and references therein). We use a trajectory from the NSM simulations of S. Rosswog [20, 21] with recommended electron fraction of $Y_e = 0.035$. For nuclear reaction and decay data, we start with JINA Reaclib nuclear reaction database [22], adding relevant r-process nuclear data calculated as self-consistently as possible. We calculate neutron-capture and neutron-induced fission rates self-consistently from input nuclear masses using the Los Alamos National Laboratory statistical Hauser-Feshbach code [23]. Where available, known masses and decay rates are used from the Atomic Mass Evaluation and Nubase2016 [24]. (For details, see [19].) We test four different variations on the nuclear physics input to test the sensitivity of actinide production on nuclear data:

(i) Baseline: FRDM2012 masses, with β-decay rates from [25], and a simple, symmetric description for fission fragments for all fission channels.

(ii) DZ: As in the baseline case, but change nuclear masses according to the Duflo-Zuker mass model [26]. Reaction and decay rates are recalculated using these masses, with β-strength functions and fission barrier heights kept the same as in the baseline case.

(iii) K&T: As in the baseline case, but change the fission fragment distribution to the

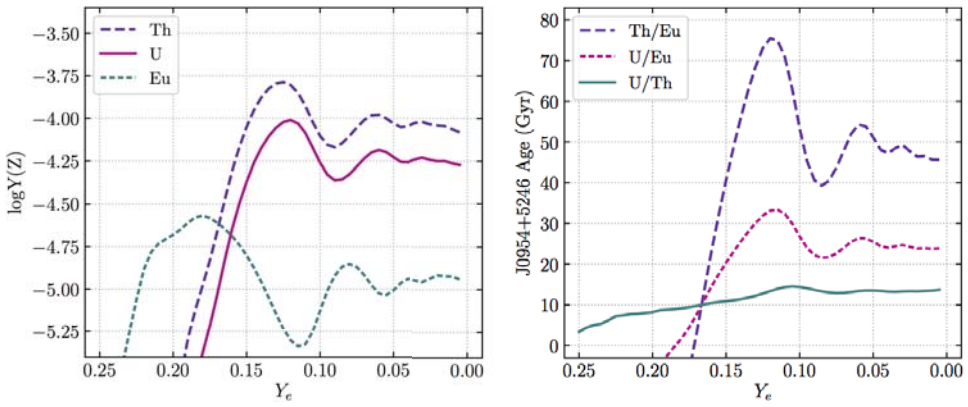

Figure 3. Left: final Th, U, and Eu abundances as a function of initial Y_e. Right: ages of J0954+5246 calculated using the corresponding Th/Eu, U/Eu, and U/Th production ratios at each Y_e. Note that only one Y_e value gives consistent ages.

double-Gaussian distributions described by [27].

(iv) Marketin: As in the baseline case, but change the β-decay rates from [25] to those of [28].

Figure 2 shows the final (1 Gyr) isotopic and elemental abundances for each of these four cases. The elemental patterns are also compared to the abundances of an extremely actinide-boost star, J0954+5246 [7]. In every case, the actinides are overproduced compared to the observations, and the production of Eu varies dramatically. Next, we test if astrophysical variations rather than differences in the assumed nuclear properties of nuclei far from stability can produce abundances in agreement with actinide-boost stars.

3. Astrophysical Variations

The initial electron fraction, Y_e, taking any value between 0 and 1, describes the initial composition of the nuclear material involved in the r-process, with a lower Y_e meaning more neutron-rich, and a higher Y_e more proton-rich. In this section, we change the initial nuclear composition by varying the Y_e to investigate the sensitivity of actinide and lanthanide production on this astrophysical parameter. For each case of nuclear input, we run 50 nucleosynthesis network simulations, changing the initial Y_e from 0.005 to 0.250 in steps of 0.005. Next, we take the final abundances from each of these simulations and use them as the initial production ratios to calculate ages for the actinide-boost star, J0954+5246. Figure 3 shows the final abundances and stellar ages calculated at each initial Y_e. Only one value of Y_e produces consistent ages, agreeing on an age of 11 Gyr (10 Gyr plus the 1 Gyr end-time of the nucleosynthesis simulations). This particular Y_e is at about 0.17, much greater than the suggested value of 0.035 from the hydrodynamical simulation of the dynamical ejecta.

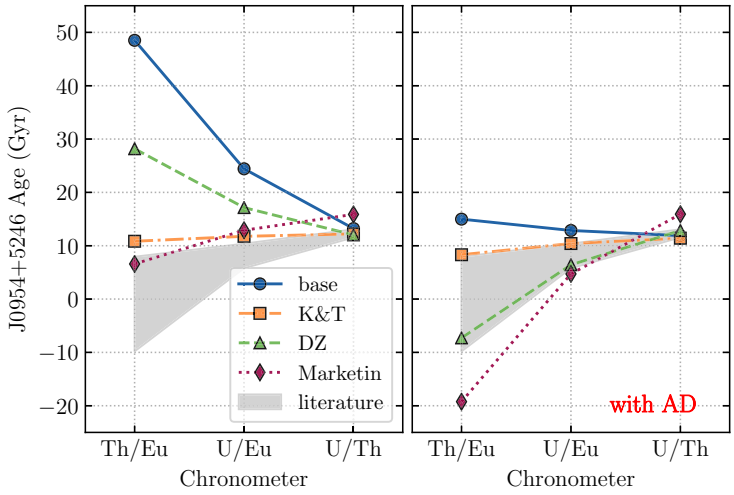

Figure 4. Left: ages for the actinide-boost star J0954+5246 calculated using Equations 1–3 at a Y_e of 0.035 for four choices of nuclear input. Right: the same ages, this time considering a distribution of Y_e described by the AD model.

4. Actinide Dilution

Rather than finding one Y_e and one particular set of nuclear input needed to explain the actinide-boost, we consider a combination of Y_e in a method we call "Actinide-Dilution" (AD). In the AD model, we choose a double-Gaussian distribution of Y_e, where one Gaussian represents the tidal/dynamical ejecta of an NSM, and the other the mass ejected by the disk wind. Fits for the Gaussians are based on the models of [29] using SFHO for the dynamical ejecta and the H000 model of [30] for the disk wind. Then, the amplitudes of the Gaussians are adjusted such that the mass ratio between the dynamical and wind ejecta components is $m_{\rm w}/m_{\rm dyn} = 3$, which is what some studies suggest as the corresponding ejecta ratio from GW170817 [31, 32]. In summary, this method generates a double-Gaussian approximation for the distribution of NSM ejecta as a function of Y_e.

Since the actinides are unstable, applying Equations 1–3 will reveal if the production ratios from the nuclear variations (i.e., using the abundances from Figure 2) are a reasonable descriptor of the r-process that produced the material in actinide-boost stars. The left panel of Figure 4 shows the three ages calculated from Equations 1–3 using the final abundances for each choice of nuclear physics input. Recall that for the simulation to accurately describe the r-process event responsible for the actinide-boost star, all three ages must agree. Using just the $Y_e = 0.035$ abundances, only one set of nuclear data generates consistent ages: the K&T case. However, in this case, the broad fission fragment distribution is a poor match to the rest of the stellar abundance pattern of the actinide-boost star J0954+5246, and the Th/Eu and U/Eu are only consistent due to the artificially enhanced Eu abundances. Using β-decay rates from Marketin produces the next best set of consistent ages. However, the U/Th age (which is well-constrained

by observations and other theoretical studies of production ratios) leads to an age of about 17 Gyr—much greater than the age of the Universe.

The right panel of Figure 4 shows the ages calculated from the combination of Y_e according to the AD model. After applying the AD distribution of Y_e (instead of a single Y_e) to each of the nuclear variations considered, we find that the actinide abundance and relative actinide-to-lanthanide ratio are lowered to levels that are roughly in agreement with abundances derived from observations of metal-poor stars. The DZ mass model fared better than the FRDM2012 model in the single-Y_e case, but leads to negative ages with the AD model. Using the β-decay rates of Marketin also leads to negative Th/Eu ages and the anomalously high U/Th is not fixed by a combination of Y_e. Stellar ages calculated from production ratios using the FRDM2012 mass model (the baseline case) generally lead to the most realistic and consistent ages. Next, we take the AD model further by finding a description for the mass distribution as a function of Y_e that fits different actinide variations.

5. Actinide Dilution with Matching

In this section, we extend the Actinide-Dilution model to more explicitly match an input abundance pattern in a new method we call the "Actinide-Dilution with Matching" (ADM) model. As a requirement for the model, the star must have a Th abundance determined, as well as Dy and Zr, representing the lanthanides and first r-process peak, respectively. We use the abundances from the same actinide-boost star as above.

Three constraints are supplied to the ADM model: the relative Zr/Dy, Th/Dy, and U/Th abundances. The Zr/Dy and Th/Dy abundances ratios are taken from the reported values of the actinide-boost star. Not all stars have a reported measurement for U, so we choose the production ratio of $\log \epsilon(\mathrm{U/Th}) = -0.25$ for this constraint. Next, we run a series of simulations using PRISM and vary the initial Y_e between 0.005 and 0.450, similar to the calculations in Section 3, this time instead using a trajectory consistent with the disk wind from a merger remnant instead of a dynamical trajectory (see [33] for details). We also vary the input mass model, repeating all simulations with the Duflo-Zuker and the Hartree-Fock-Bogoliubov (HFB) [34] models after self-consistently recalculating all relevant nuclear data as described in Section 2. Now, we have a set of final abundance patterns calculated across a range of Y_e values for three different nuclear mass models.

The ADM model randomly selects 15 values of Y_e, combines the final associated abundances, then tests if the Zr/Dy, Th/Dy, and U/Th ratios agree with the input constraints from observationally derived abundances. If all three are within about 0.2 dex of the input constraints, the set of Y_e is kept and added to a cumulative mass distribution. This set is then one realization of the ejecta from the event that could have produced the input abundances. Otherwise, the model resamples a different set of 15 and tries again. The model stops after it has accumulated 100 successes, totaling 1500 summed abundance patterns and a full distribution of Y_e.

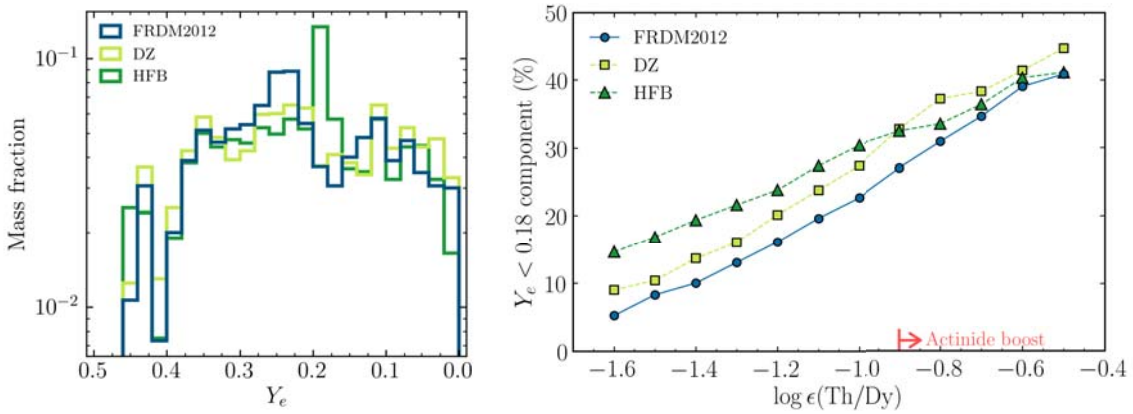

Figure 5. Left: mass fractions of r-process ejecta predicted by the ADM model using abundances from J0954+5246 as matching constrains with three different nuclear mass models. Right: the percentage of very low-Y_e mass that may be ejected from an r-process site in order to produce the specified actinide-to-lanthanide abundance ratio ($\log \epsilon$(Th/Dy)).

The left panel of Figure 5 shows the mass distribution results for each mass model applied to the abundances for J0954+5246. This mass distribution describes how the ejecta from an r-process event could have been distributed in order to match the input abundances. We also test other input actinide values, rerunning the ADM model using a range of $\log \epsilon$(Th/Dy) (actinide-to-lanthanide) ratios that spans over all current observationally derived $\log \epsilon$(Th/Dy) abundances, including actinide-poor and actinide-boost. Then, we look at the total contribution from the very neutron-rich component ($Y_e < 0.18$). The right panel of Figure 5 shows the percentage of the total ejecta mass that begins the r-process at very neutron-rich values for certain input relative actinide abundances. The smoothly increasing trend for the low-Y_e component as a function of actinide-to-lanthanide ratio is similar for each mass model, with about a 10% maximum difference between the three models. In the HFB case, the actinides are not produced as abundantly as in the FRDM2012 or DZ cases, and therefore more low-Y_e material is allowed to contribute to the total, final actinide abundance. However, the difference between an actinide-poor case ($\log \epsilon$(Th/Dy) < -1.20) and an actinide-boost case ($\log \epsilon$(Th/Dy) > -0.90) is only about 15%. In other words, an r-process event must eject roughly 15% more of its material at very low values of Y_e in order to change its produced abundances from actinide-poor to actinide-rich.

6. Conclusions

We have investigated the source of the stellar actinide-boost phenomenon to uncover whether this boost has an origin in key nuclear data or indicates some distinct r-process site. In a very neutron-rich environment, such as the tidal ejecta from an NSM, we found that no single choice of nuclear input produces consistent radioactive decay ages for the very actinide-boost star, J0954+5246. Instead, the actinide-to-lanthanide ratio

is always overproduced compared to the observational abundance ratios, indicating the need for the actinides to be diluted by a lanthanide-rich, actinide-poor component of the r-process ejecta. Such a component could be explained by the moderately neutron-rich accretion disk wind from an NSM remnant [35]. The AD model builds such a possible ejecta distribution which dilutes the actinides of a tidal-only ejecta scenario with a lanthanide-rich wind component. Borrowing values from both literature studies of NSM ejecta and estimates from the observed kilonova associated with GW170817, the AD model produces a better match to the observed Th/Eu abundance ratio of an actinide-boost star, especially by using the FRDM2012 mass model with consistent nuclear data.

Developing this model further, we used the ADM model to build empirical ejecta distributions describing how the material from an r-process event would be distributed in order to match actinide-boost abundances. The results of this model indicate a significant, but non-dominant, component of the ejecta must have very low Y_e in order to explain actinide-boost abundances. However, from the smooth growth of the neutron-rich portion of the r-process ejecta in Figure 5, there appears to be no distinct difference between actinide-boost cases and stars without an actinide-boost, indicating there is no need for a separate r-process progenitor type for actinide-boost stars. Instead, the same type of r-process site can produce either an actinide-poor, actinide-normal, or actinide-boost case depending on the morphology of the ejecta. For example, this can be accommodated in an NSM scenario if the merger event ejects more (actinide-boost) or less (actinide-poor) dynamical/tidal ejecta, which tend to be more neutron-rich than the wind ejecta.

References

[1] E. M. Burbidge, G. R. Burbidge, W. A. Fowler, and F. Hoyle. Synthesis of the Elements in Stars. *Rev. Mod. Phys.* , 29:547–650, 1957.

[2] A. G. W. Cameron. Nuclear Reactions in Stars and Nucleogenesis. *PASP* , 69:201, June 1957.

[3] C. Sneden, J. J. Cowan, and R. Gallino. Neutron-Capture Elements in the Early Galaxy. *ARA&A* , 46:241–288, September 2008.

[4] I. U. Roederer, G. W. Preston, I. B. Thompson, S. A. Shectman, C. Sneden, G. S. Burley, and D. D. Kelson. A Search for Stars of Very Low Metal Abundance. VI. Detailed Abundances of 313 Metal-poor Stars. *AJ* , 147:136, June 2014.

[5] V. Hill, N. Christlieb, T. C. Beers, P. S. Barklem, K.-L. Kratz, B. Nordström, B. Pfeiffer, and K. Farouqi. The Hamburg/ESO R-process Enhanced Star survey (HERES). XI. The highly r-process-enhanced star CS 29497-004. *A&A* , 607:A91, November 2017.

[6] C. Siqueira Mello, M. Spite, B. Barbuy, F. Spite, E. Caffau, V. Hill, S. Wanajo, F. Primas, B. Plez, R. Cayrel, J. Andersen, B. Nordström, C. Sneden, T. C. Beers, P. Bonifacio, P. François, and P. Molaro. First stars. XVI. HST/STIS abundances of heavy elements in the uranium-rich metal-poor star CS 31082-001. *A&A* , 550:A122, February 2013.

[7] E. M. Holmbeck, T. C. Beers, I. U. Roederer, V. M. Placco, T. T. Hansen, C. M. Sakari, C. Sneden, C. Liu, Y. S. Lee, J. J. Cowan, and A. Frebel. The R-Process Alliance: 2MASS J09544277+5246414, the Most Actinide-enhanced R-II Star Known. *ApJL* , 859:L24, June 2018.

[8] L. Mashonkina, N. Christlieb, P. S. Barklem, V. Hill, T. C. Beers, and A. Velichko. The

Hamburg/ESO R-process enhanced star survey (HERES). V. Detailed abundance analysis of the r-process enhanced star HE 2327-5642. *A&A* , 516:A46, June 2010.

[9] L. Mashonkina, N. Christlieb, and K. Eriksson. The Hamburg/ESO R-process Enhanced Star survey (HERES). X. HE 2252-4225, one more r-process enhanced and actinide-boost halo star. *A&A* , 569:A43, September 2014.

[10] V. M. Placco, E. M. Holmbeck, A. Frebel, T. C. Beers, R. A. Surman, A. P. Ji, R. Ezzeddine, S. D. Points, C. C. Kaleida, T. T. Hansen, C. M. Sakari, and A. R. Casey. RAVE J203843.2-002333: The First Highly R-process-enhanced Star Identified in the RAVE Survey. *ApJ* , 844:18, July 2017.

[11] A. Frebel, N. Christlieb, J. E. Norris, C. Thom, T. C. Beers, and J. Rhee. Discovery of HE 1523-0901, a Strongly r-Process-enhanced Metal-poor Star with Detected Uranium. *ApJL* , 660:L117–L120, May 2007.

[12] C. M. Sakari, V. M. Placco, T. Hansen, E. M. Holmbeck, T. C. Beers, A. Frebel, I. U. Roederer, K. A. Venn, G. Wallerstein, C. E. Davis, E. M. Farrell, and D. Yong. The r-process Pattern of a Bright, Highly r-process-enhanced Metal-poor Halo Star at [Fe/H]~ -2. *ApJL* , 854:L20, February 2018.

[13] S. Wanajo, N. Itoh, Y. Ishimaru, S. Nozawa, and T. C. Beers. The r-Process in the Neutrino Winds of Core-Collapse Supernovae and U-Th Cosmochronology. *ApJ* , 577:853–865, October 2002.

[14] K. Farouqi, K.-L. Kratz, B. Pfeiffer, T. Rauscher, F.-K. Thielemann, and J. W. Truran. Charged-particle and Neutron-capture Processes in the High-entropy Wind of Core-collapse Supernovae. *ApJ* , 712:1359–1377, April 2010.

[15] B. P. Abbott, R. Abbott, T. D. Abbott, F. Acernese, K. Ackley, C. Adams, T. Adams, P. Addesso, R. X. Adhikari, V. B. Adya, and et al. GW170817: Observation of Gravitational Waves from a Binary Neutron Star Inspiral. *Phys. Rev. Lett.* , 119(16):161101, October 2017.

[16] P. S. Cowperthwaite, E. Berger, V. A. Villar, B. D. Metzger, M. Nicholl, R. Chornock, P. K. Blanchard, W. Fong, R. Margutti, M. Soares-Santos, K. D. Alexander, S. Allam, J. Annis, D. Brout, D. A. Brown, R. E. Butler, H.-Y. Chen, H. T. Diehl, Z. Doctor, M. R. Drout, T. Eftekhari, B. Farr, D. A. Finley, R. J. Foley, J. A. Frieman, C. L. Fryer, J. García-Bellido, M. S. S. Gill, J. Guillochon, K. Herner, D. E. Holz, D. Kasen, R. Kessler, J. Marriner, T. Matheson, E. H. Neilsen, Jr., E. Quataert, A. Palmese, A. Rest, M. Sako, D. M. Scolnic, N. Smith, D. L. Tucker, P. K. G. Williams, E. Balbinot, J. L. Carlin, E. R. Cook, F. Durret, T. S. Li, P. A. A. Lopes, A. C. C. Lourenço, J. L. Marshall, G. E. Medina, J. Muir, R. R. Muñoz, M. Sauseda, D. J. Schlegel, L. F. Secco, A. K. Vivas, W. Wester, A. Zenteno, Y. Zhang, T. M. C. Abbott, M. Banerji, K. Bechtol, A. Benoit-Lévy, E. Bertin, E. Buckley-Geer, D. L. Burke, D. Capozzi, A. Carnero Rosell, M. Carrasco Kind, F. J. Castander, M. Crocce, C. E. Cunha, C. B. D'Andrea, L. N. da Costa, C. Davis, D. L. DePoy, S. Desai, J. P. Dietrich, A. Drlica-Wagner, T. F. Eifler, A. E. Evrard, E. Fernandez, B. Flaugher, P. Fosalba, E. Gaztanaga, D. W. Gerdes, T. Giannantonio, D. A. Goldstein, D. Gruen, R. A. Gruendl, G. Gutierrez, K. Honscheid, B. Jain, D. J. James, T. Jeltema, M. W. G. Johnson, M. D. Johnson, S. Kent, E. Krause, R. Kron, K. Kuehn, N. Nuropatkin, O. Lahav, M. Lima, H. Lin, M. A. G. Maia, M. March, P. Martini, R. G. McMahon, F. Menanteau, C. J. Miller, R. Miquel, J. J. Mohr, E. Neilsen, R. C. Nichol, R. L. C. Ogando, A. A. Plazas, N. Roe, A. K. Romer, A. Roodman, E. S. Rykoff, E. Sanchez, V. Scarpine, R. Schindler, M. Schubnell, I. Sevilla-Noarbe, M. Smith, R. C. Smith, F. Sobreira, E. Suchyta, M. E. C. Swanson, G. Tarle, D. Thomas, R. C. Thomas, M. A. Troxel, V. Vikram, A. R. Walker, R. H. Wechsler, J. Weller, B. Yanny, and J. Zuntz. The Electromagnetic Counterpart of the Binary Neutron Star Merger LIGO/Virgo GW170817. II. UV, Optical, and Near-infrared Light Curves and Comparison to Kilonova Models. *ApJL* , 848:L17, October 2017.

[17] M. R. Drout, A. L. Piro, B. J. Shappee, C. D. Kilpatrick, J. D. Simon, C. Contreras, D. A. Coulter, R. J. Foley, M. R. Siebert, N. Morrell, K. Boutsia, F. Di Mille, T. W.-S. Holoien, D. Kasen,

J. A. Kollmeier, B. F. Madore, A. J. Monson, A. Murguia-Berthier, Y.-C. Pan, J. X. Prochaska, E. Ramirez-Ruiz, A. Rest, C. Adams, K. Alatalo, E. Bañados, J. Baughman, T. C. Beers, R. A. Bernstein, T. Bitsakis, A. Campillay, T. T. Hansen, C. R. Higgs, A. P. Ji, G. Maravelias, J. L. Marshall, C. M. Bidin, J. L. Prieto, K. C. Rasmussen, C. Rojas-Bravo, A. L. Strom, N. Ulloa, J. Vargas-González, Z. Wan, and D. D. Whitten. Light curves of the neutron star merger GW170817/SSS17a: Implications for r-process nucleosynthesis. *Science*, 358:1570–1574, December 2017.

[18] D. Kasen, B. Metzger, J. Barnes, E. Quataert, and E. Ramirez-Ruiz. Origin of the heavy elements in binary neutron-star mergers from a gravitational-wave event. *Nature* , 551:80–84, November 2017.

[19] E. M. Holmbeck, T. M. Sprouse, M. R. Mumpower, N. Vassh, R. Surman, T. C. Beers, and T. Kawano. Actinide Production in the Neutron-rich Ejecta of a Neutron Star Merger. *ApJ* , 870:23, January 2019.

[20] S. Rosswog, T. Piran, and E. Nakar. The multimessenger picture of compact object encounters: binary mergers versus dynamical collisions. *MNRAS* , 430:2585–2604, April 2013.

[21] T. Piran, E. Nakar, and S. Rosswog. The electromagnetic signals of compact binary mergers. *MNRAS* , 430:2121–2136, April 2013.

[22] R. H. Cyburt, A. M. Amthor, R. Ferguson, Z. Meisel, K. Smith, S. Warren, A. Heger, R. D. Hoffman, T. Rauscher, A. Sakharuk, H. Schatz, F. K. Thielemann, and M. Wiescher. The jina reaclib database: Its recent updates and impact on type-i x-ray bursts. *ApJS* , 189(1):240, 2010.

[23] T. Kawano, R. Capote, S. Hilaire, and P. Chau Huu-Tai. Statistical Hauser-Feshbach theory with width-fluctuation correction including direct reaction channels for neutron-induced reactions at low energies. *Phys. Rev. C.* , 94(1):014612, July 2016.

[24] G. Audi, F. G. Kondev, M. Wang, W. J. Huang, and S. Naimi. The NUBASE2016 evaluation of nuclear properties. *Chinese Physics C*, 41(3):030001, March 2017.

[25] P. Möller, M. R. Mumpower, T. Kawano, and W. D. Myers. Nuclear properties for astrophysical and radioactive-ion-beam applications (II). *Atomic Data and Nuclear Data Tables*, 125:1–192, January 2019.

[26] J. Duflo and A. P. Zuker. Microscopic mass formulas. *Phys. Rev. C.* , 52:R23–R27, July 1995.

[27] T. Kodama and K. Takahashi. R-process nucleosynthesis and nuclei far from the region of β-stability. *Nucl. Phys. A*, 239:489–510, March 1975.

[28] T. Marketin, L. Huther, and G. Martínez-Pinedo. Large-scale evaluation of β-decay rates of r-process nuclei with the inclusion of first-forbidden transitions. *Phys. Rev. C.* , 93:025805, Feb 2016.

[29] L. Bovard, D. Martin, F. Guercilena, A. Arcones, L. Rezzolla, and O. Korobkin. r - process nucleosynthesis from matter ejected in binary neutron star mergers. *Phys. Rev. D.* , 96(12):124005, December 2017.

[30] J. Lippuner, R. Fernández, L. F. Roberts, F. Foucart, D. Kasen, B. D. Metzger, and C. D. Ott. Signatures of hypermassive neutron star lifetimes on r-process nucleosynthesis in the disc ejecta from neutron star mergers. *MNRAS* , 472:904–918, November 2017.

[31] S. Rosswog, J. Sollerman, U. Feindt, A. Goobar, O. Korobkin, C. Fremling, and M. Kasliwal. The first direct double neutron star merger detection: implications for cosmic nucleosynthesis. *ArXiv e-prints*, October 2017.

[32] M. Tanaka, Y. Utsumi, P. A. Mazzali, N. Tominaga, M. Yoshida, Y. Sekiguchi, T. Morokuma, K. Motohara, K. Ohta, K. S. Kawabata, F. Abe, K. Aoki, Y. Asakura, S. Baar, S. Barway, I. A. Bond, M. Doi, T. Fujiyoshi, H. Furusawa, S. Honda, Y. Itoh, M. Kawabata, N. Kawai, J. H. Kim, C.-H. Lee, S. Miyazaki, K. Morihana, H. Nagashima, T. Nagayama, T. Nakaoka, F. Nakata, R. Ohsawa, T. Ohshima, H. Okita, T. Saito, T. Sumi, A. Tajitsu, J. Takahashi, M. Takayama, Y. Tamura, I. Tanaka, T. Terai, P. J. Tristram, N. Yasuda, and T. Zenko. Kilonova from post-merger ejecta as an optical and near-Infrared counterpart of GW170817. *PASJ* , 69:102, December 2017.

[33] E. M. Holmbeck, A. Frebel, G. C. McLaughlin, M. R. Mumpower, T. M. Sprouse, and R. Surman. Actinide-rich and Actinide-poor r-process-enhanced Metal-poor Stars Do Not Require Separate r-process Progenitors. *ApJ* , 881(1):5, Aug 2019.

[34] S. Goriely, N. Chamel, and J. M. Pearson. Skyrme-Hartree-Fock-Bogoliubov Nuclear Mass Formulas: Crossing the 0.6MeV Accuracy Threshold with Microscopically Deduced Pairing. *Phys. Rev. Lett.* , 102(15):152503, April 2009.

[35] Jonah M. Miller, Benjamin R. Ryan, Joshua C. Dolence, Adam Burrows, Christopher J. Fontes, Christopher L. Fryer, Oleg Korobkin, Jonas Lippuner, Matthew R. Mumpower, and Ryan T. Wollaeger. Full transport model of GW170817-like disk produces a blue kilonova. *Phys. Rev. D.* , 100(2):023008, Jul 2019.